Supplementary Material

Revealing the Reversal of Anomalous Hall Effect and Exchange Bias-like Effect in Single-Phase Perpendicularly Magnetized $NiCo_2O_4$ Epitaxial Films

Penghua Kang,[1,2] Guowei Zhou,[2,3,a)] Jiashuo Liang,[1] Guoxiu Ren,[2] Jiahui Ji,[2] Liying Wang,[1] Chao Jin[1,a)] and Xiaohong Xu[2,3,a)]

AFFILIATIONS

[1]Tianjin Key Laboratory of Low Dimensional Materials Physics and Processing Technology, School of Science, Tianjin University, Tianjin 300354, China.

[2]School of Chemistry and Materials Science, Key Laboratory of Magnetic Molecules and Magnetic Information Materials, Ministry of Education, Shanxi Normal University, Taiyuan 030006, China

[3]Research Institute of Materials Science of Shanxi Normal University & Collaborative Innovation Center for Advanced Permanent Magnetic Materials and Technology, Taiyuan 030006, China

[a)]Authors to whom correspondence should be addressed: zhougw@sxnu.edu.cn, chaojin@tju.edu.cn and xuxh@sxnu.edu.cn

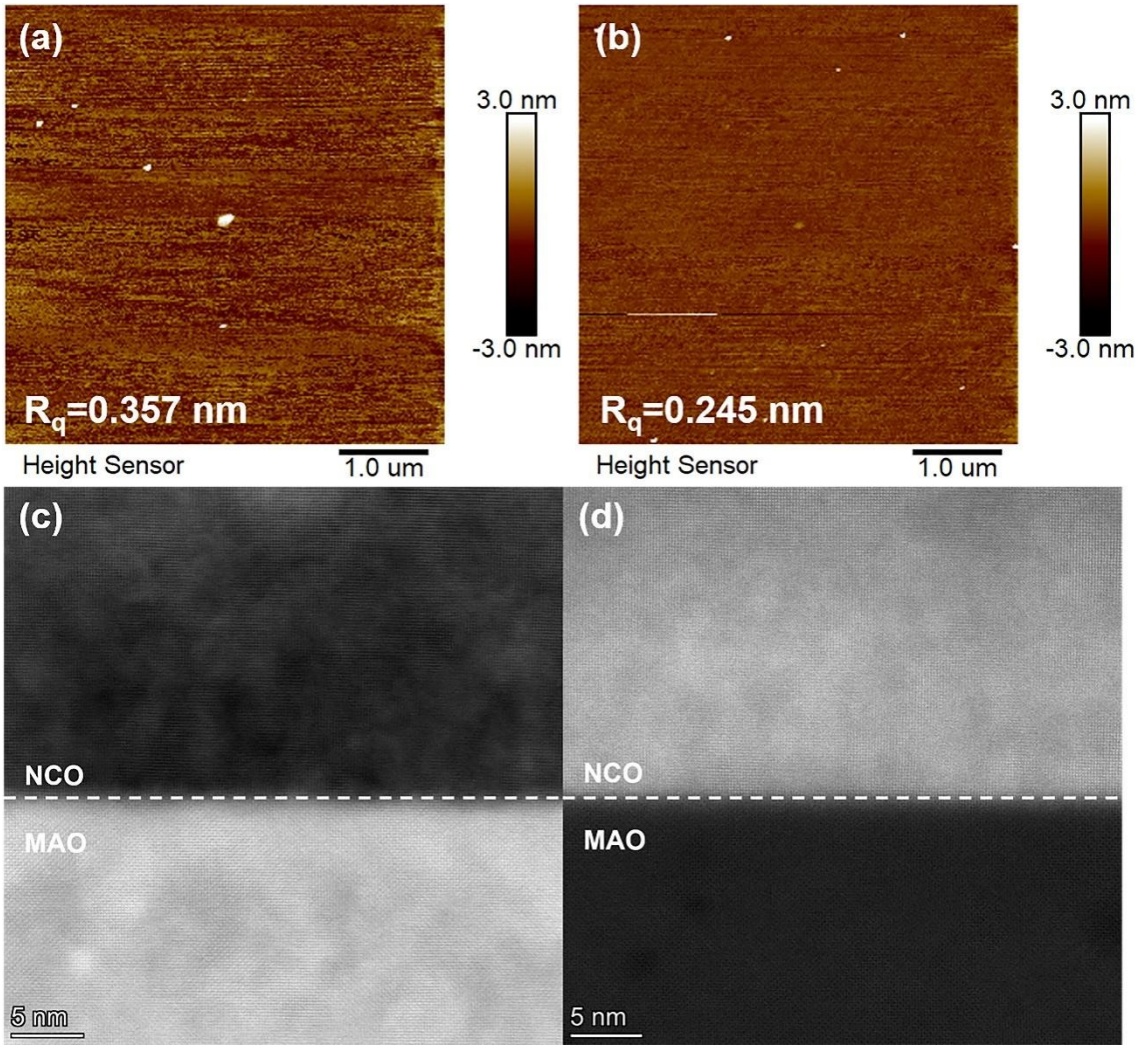

FIG. S1. Surface morphology and crystal structure of NCO films. (a,b) The AFM images of 43-nm-thick NCO films deposited at 325 and 350 °C, respectively. (c,d) The ABF-STEM and HAADF-STEM images of 43-nm-thick NCO film grown at 375 °C with a scale of 5 nm, respectively.

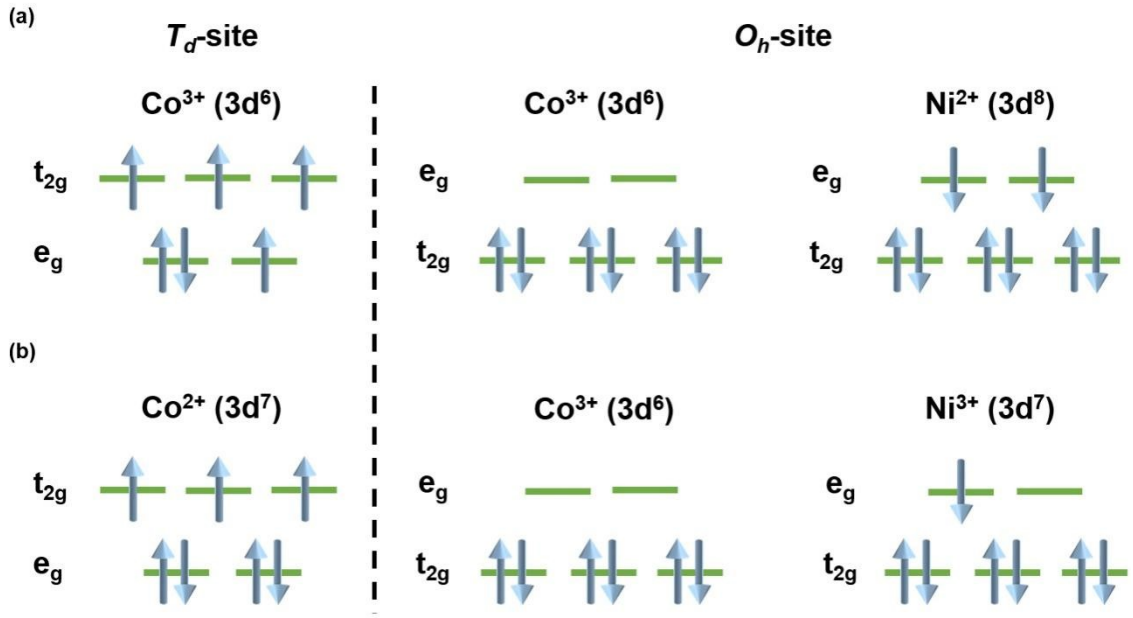

FIG. S2. Possible electronic configurations of NCO. (a) The T_d and O_h sites are occupied by Co^{3+}. The Ni^{2+} fills O_h sites. (b) The T_d and O_h sites are filled with Co^{2+} and Co^{3+}, respectively. The Ni^{3+} occupies O_h sites.

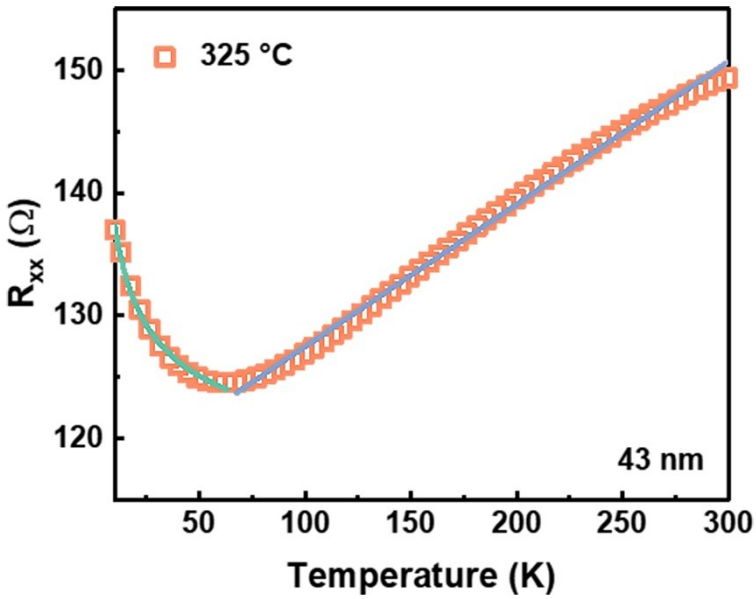

FIG. S3. Conductive mechanism of NCO films. Temperature-dependent R_{xx} of NCO film deposited 325 °C. The hollow squares denote measured values. The purple line is the R_{xx} from 60 to 300 K fitted with $\rho_{xx} = \rho_0 + AT$. The green line is the R_{xx} in the range 10 to 60 K fitted with $\rho_{xx} = \rho_0 + AT^{-\frac{1}{2}}$. It suggests that the scattering mechanism for carriers in the high temperature region is electron-phonon coupling, while it is electron-electron scattering in the low temperature regime.

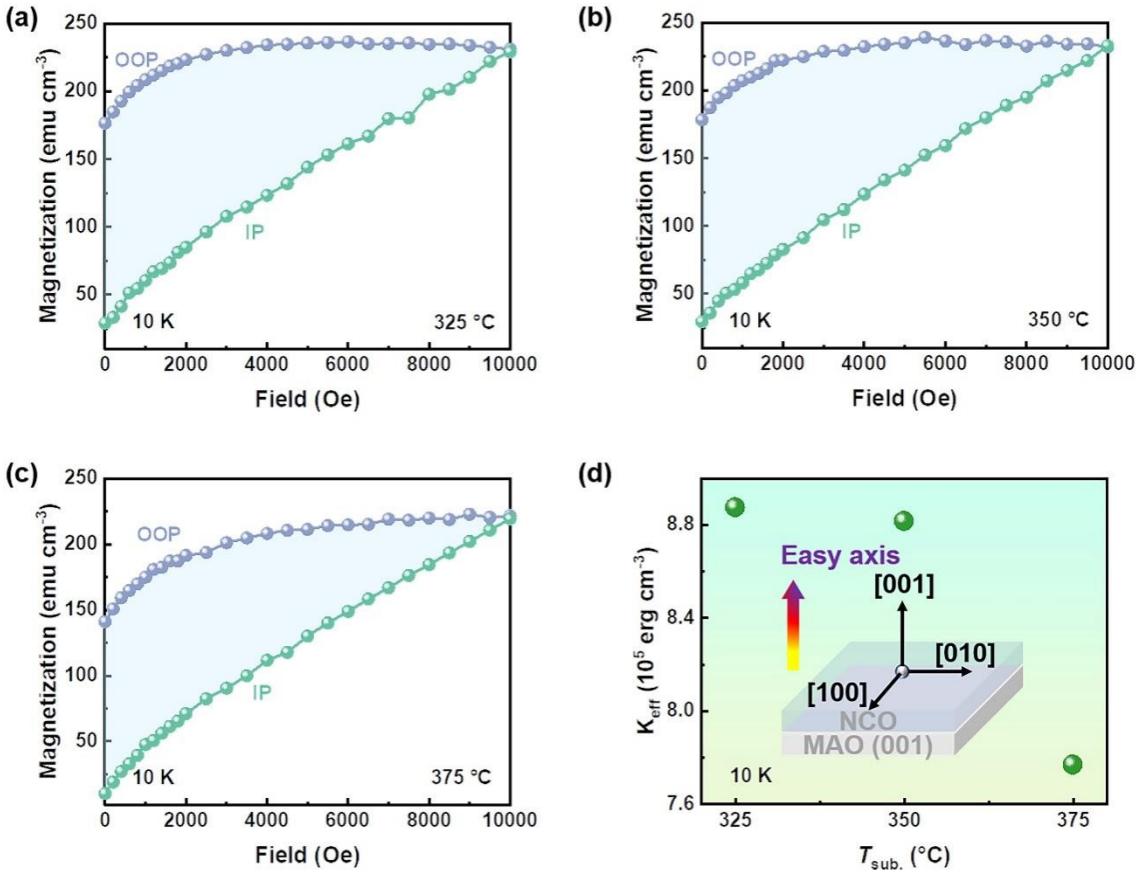

FIG. S4. Magnetic anisotropy of NCO films. (a-c) Schematic of the K_{eff} for the 43-nm-thick NCO films grown at 325, 350 and 375 °C, respectively. (d) The K_{eff} of 43-nm-thick NCO films prepared at different $T_{sub.}$ summarized from Figs. S3(a)-(c). The inset displays the schematic of the magnetic easy axis for NCO films grown on MAO (001) substrates.

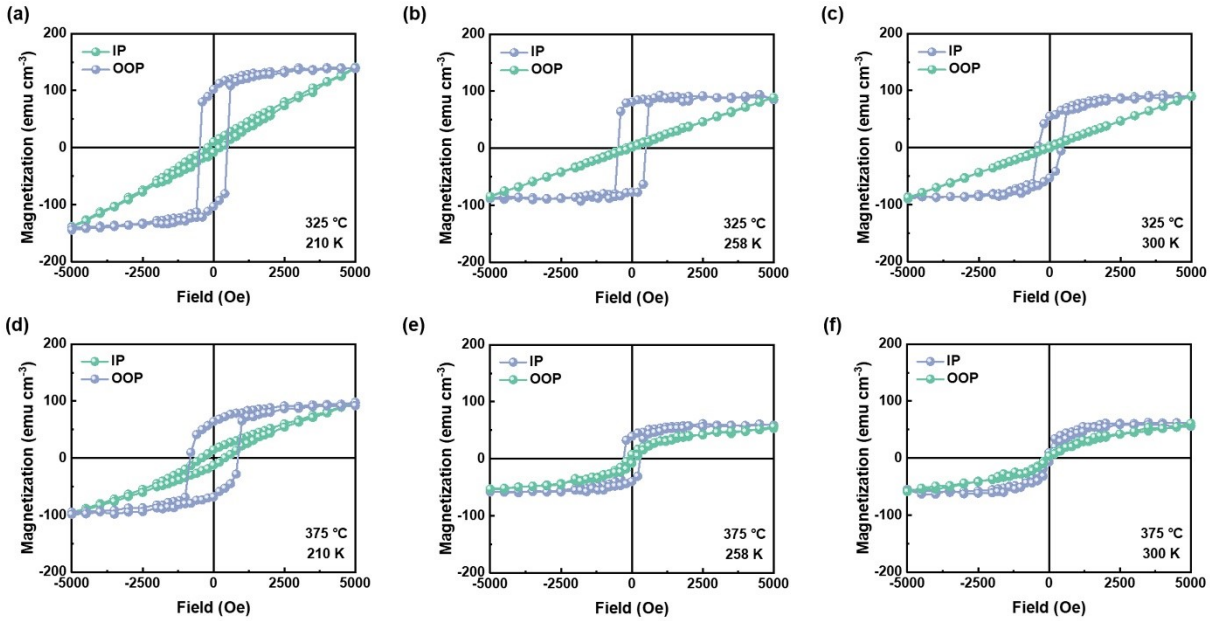

FIG. S5. Hysteresis loops at different temperatures of NCO films. (a-c) Magnetic field-dependent OOP and IP magnetization at 210, 258, and 300 K for 43-nm-thick NCO film deposited at 325 °C, respectively. (d-f) Dependence of OOP and IP magnetization on magnetic field at 210, 258, and 300 K for 43-nm-thick NCO film grown at 375 °C, respectively.

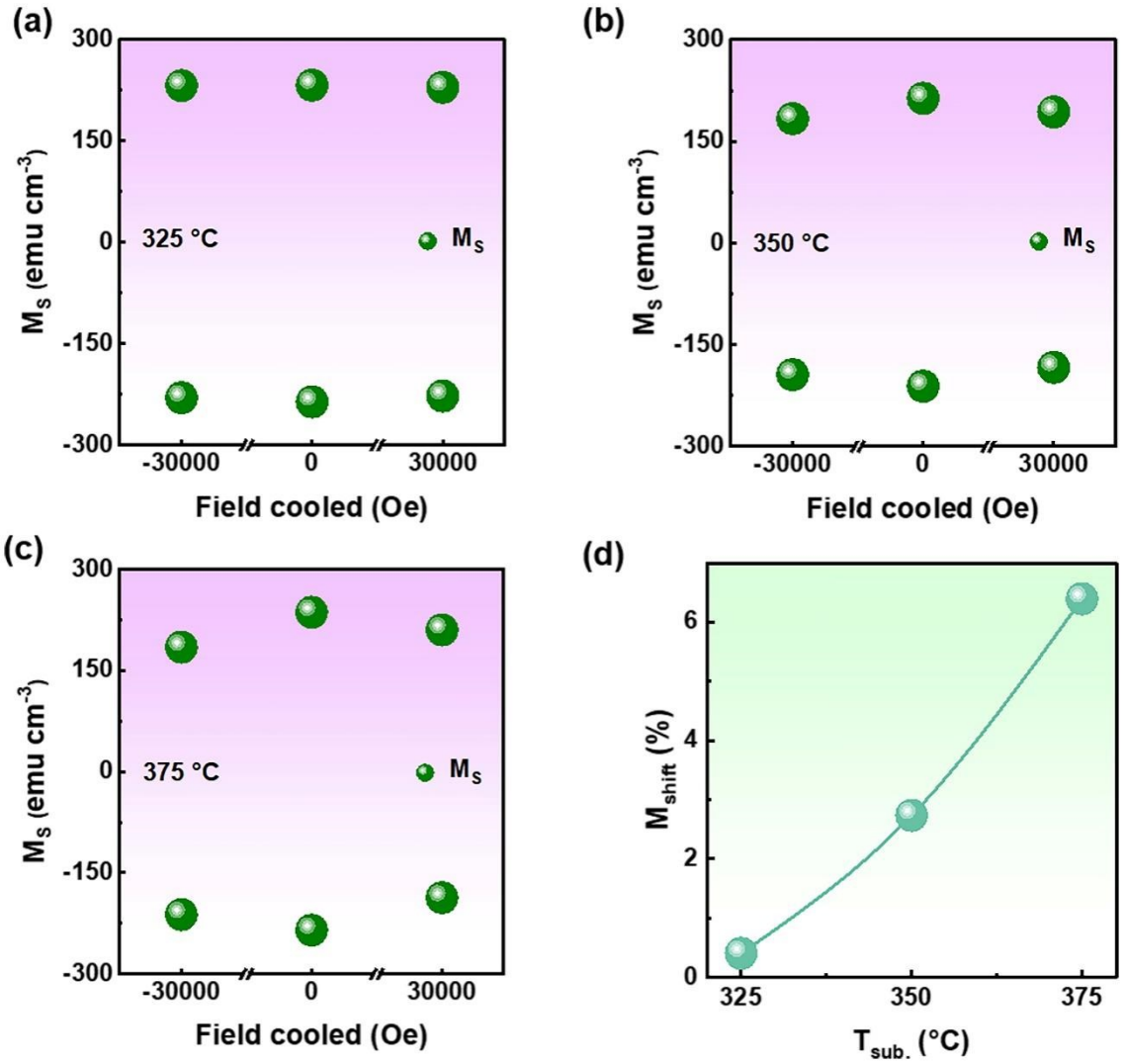

FIG. S6. EB-like effects in NCO films at low temperature. (a-c) The ^{M_S} extracted from Figs. 4(a)-(c) of 43-nm-thick NCO film deposited at 325, 350, 375 °C, respectively. (d) Dependence of M_{shift} on $T_{sub.}$ of 43-nm-thick NCO films, respectively.

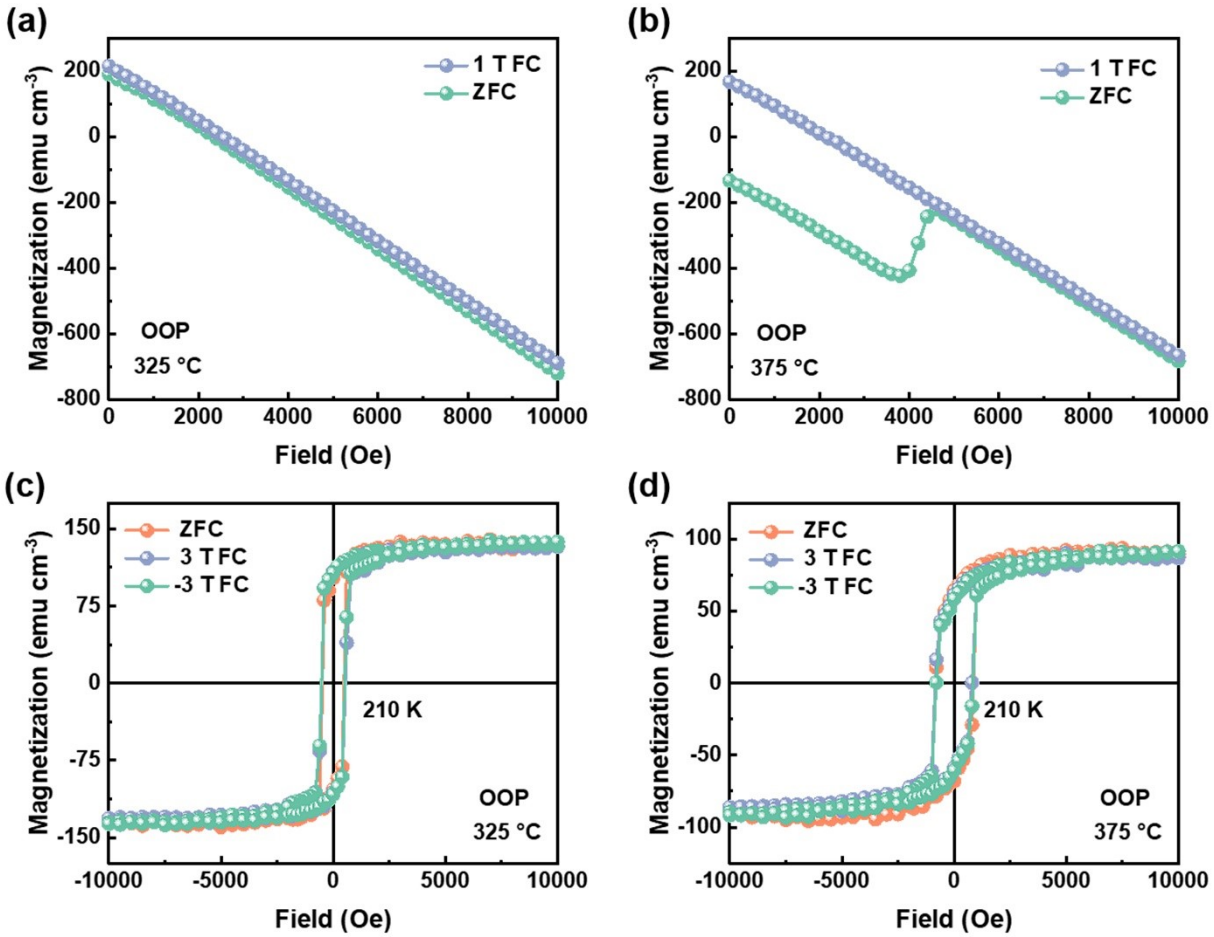

FIG. S7. (a,b) OOP initial magnetization curves under ZFC and FC processes of NCO films grown at 325 and 375 °C, respectively. The diamagnetic signal is not subtracted here. (c,d) Magnetic field-dependent OOP magnetization using the ZFC and FC protocols at 210 K for NCO films deposited at 325 and 375 °C, respectively.

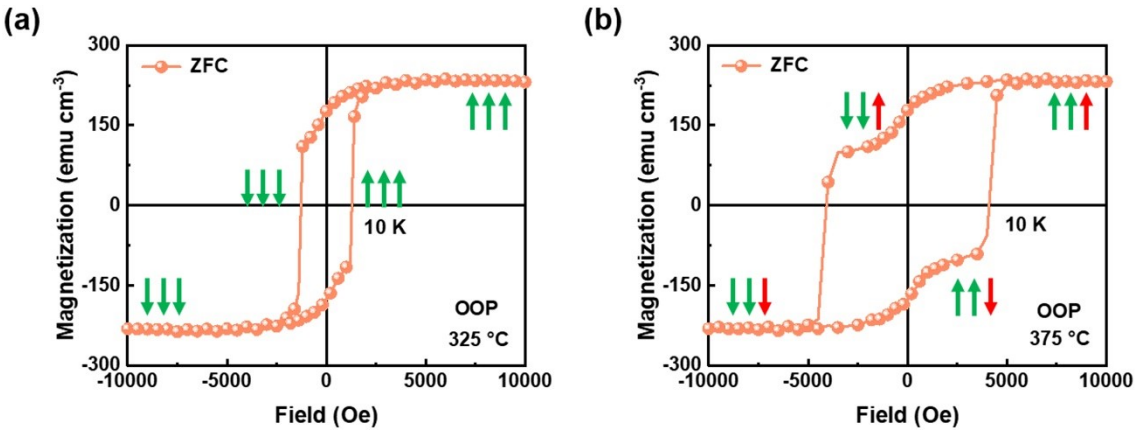

FIG. S8. a,b) Schematic illustration of the distribution of spin in NCO films deposited at 325 and 375 °C, respectively. The direction of arrows indicates the spin orientation.

For the samples prepared at 325 °C, the direction of the spin is always along the magnetic field and thus exhibits the regular M-H loop. For the NCO film prepared at 375 °C, the orientation of some of the spins did not rotate with the magnetic field when a sufficiently large magnetic field was not applied (red arrows), exhibiting localized antiferromagnetic coupling. The pinning effect of these localized antiferromagnetic coupling regions on the ferrimagnetic phase leads to the generation of EB-like effect.

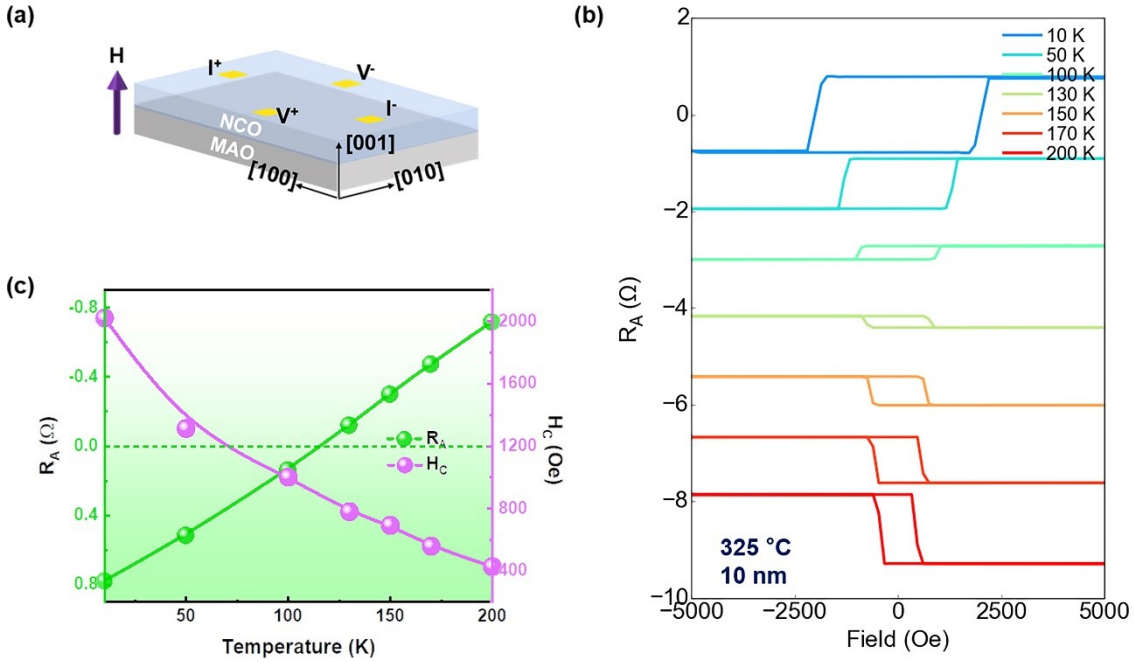

FIG. S9. AHE of the NCO film. (a) Schematic of geometric configurations for the AHE measured by the van der Pauw method. (b) Temperature-dependent AHE of 10-nm-thick NCO films prepared at 325 °C. The curves of different temperature were shifted vertically for clarity and comparability. (c) Dependence of R_A (left) and H_C (right) on temperature summarized from Fig. S9(b). The horizontal dashed line drawn denotes $R_A = 0$.

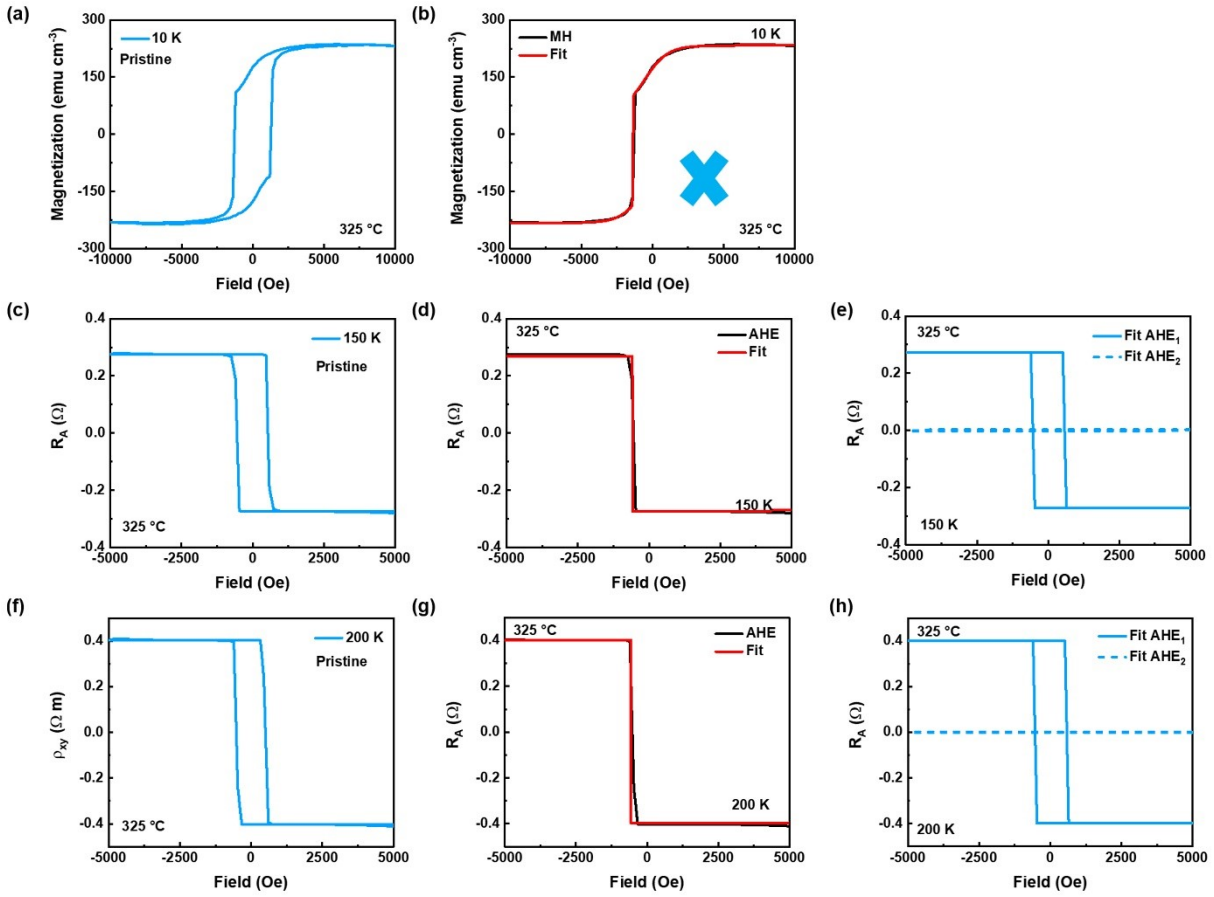

FIG. S10. Magnetic properties and AHE of NCO film. (a) Temperature-dependent OOP magnetization at 10 K for 43-nm-thick NCO film deposited at 325 °C. (b) The black line is the dependence of the magnetization on magnetic field at 10 K by sweeping from the positive to negative magnetic field. The red line is obtained by fitting Eq. 3. The blue shape in the figure indicates that the fit is not convergent. (c,f) AHE at 150 and 200 K for the sample grown at 325 °C, respectively. (d,g) The black lines are the magnetic field-dependent R_A by sweeping from the positive to negative magnetic field. The red lines are fitted to the Eq. 3. (e,h) The two components AHE_1 (solid curve) and AHE_2 (dotted curve) fitted from Fig. S10(c),(f).

Table I. The parameters obtained by fitting the hysteresis loop at 10 K of the 43-nm-thick NCO film grown at 325 °C from Eq. 3. The blue font means that the fit has not converged.

	ρ_{A_1}	H_{C_1}	H_{O_1}	ρ_{A_2}	H_{C_2}	H_{O_2}
Value	-89.3687	541.98071	-1616.41909	-143.55425	1372.52546	-21.84194
Standard Error	1.37617	20.51643	29.26389	1.32379	82299.80989	86143.49964

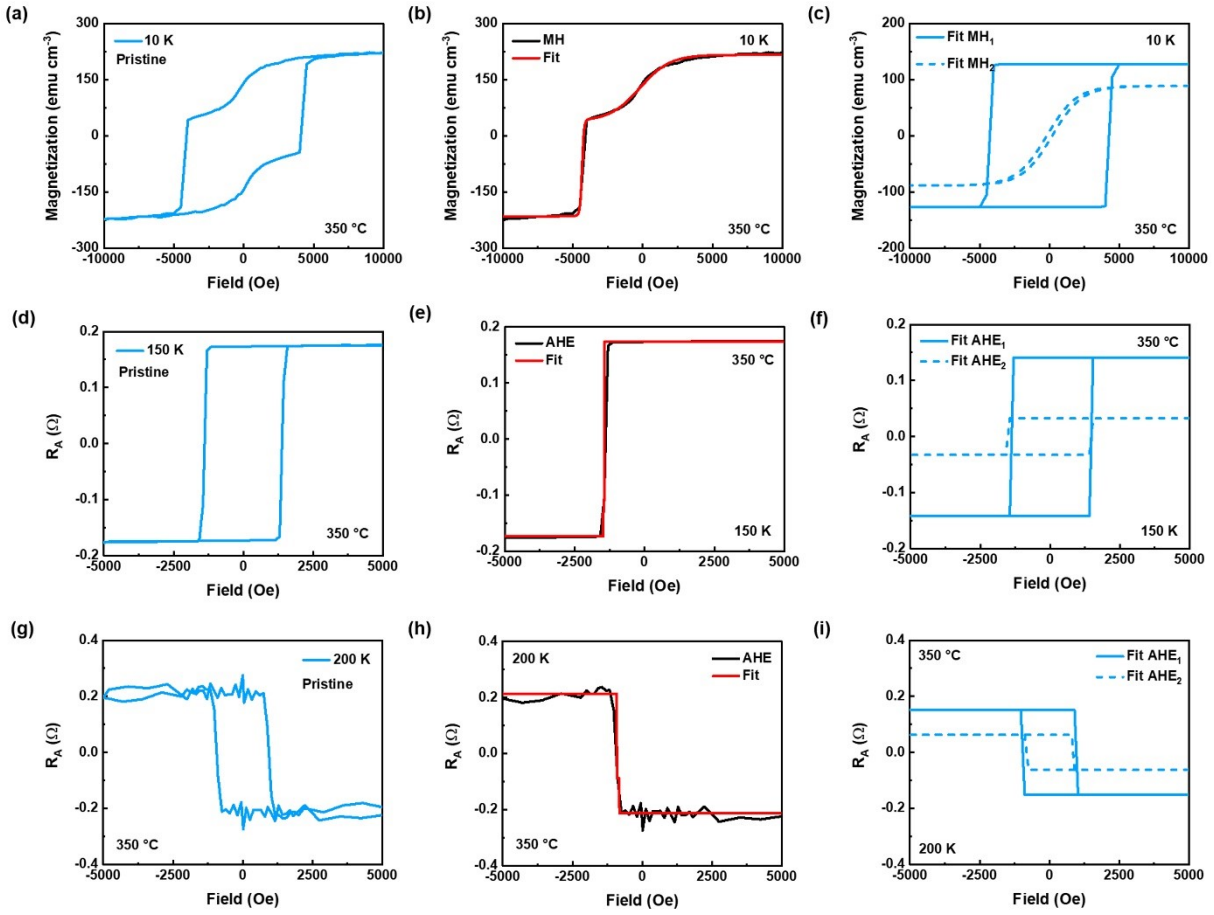

FIG. S11. Magnetic properties and AHE of NCO film. (a) Dependence of OOP magnetization on magnetic field at 10 K for 43-nm-thick NCO film deposited at 350 °C. (b) The black line is the magnetic field-dependent magnetization at 10 K by sweeping from the positive to negative magnetic field. The red line is obtained by fitting Eq. 3. (c) The two components MH_1 (solid curve) and MH_2 (dotted curve) fitted from Fig. S11(a). (d,g) AHE at 150 and 200 K for the sample grown at 350 °C, respectively. (e,h) The black lines are the magnetic field-dependent R_A by sweeping from the positive to negative magnetic field. The red lines are fitted to the Eq. 3. (f,i) The two components AHE_1 (solid curve) and AHE_2 (dotted curve) fitted from Figs. S11(d),(g).

Table II. The parameters obtained by fitting the hysteresis loop at 10 K of the 43-nm-thick NCO film grown at 350 °C from Eq. 3.

	ρ_{A_1}	H_{C_1}	H_{O_1}	ρ_{A_2}	H_{C_2}	H_{O_2}
Value	-88.60122	195.88568	-2143.44422	-127.72762	4333.584	-142.8353
Standard Error	2.30604	71.9663	105.39462	2.08343	55.46949	53.18068

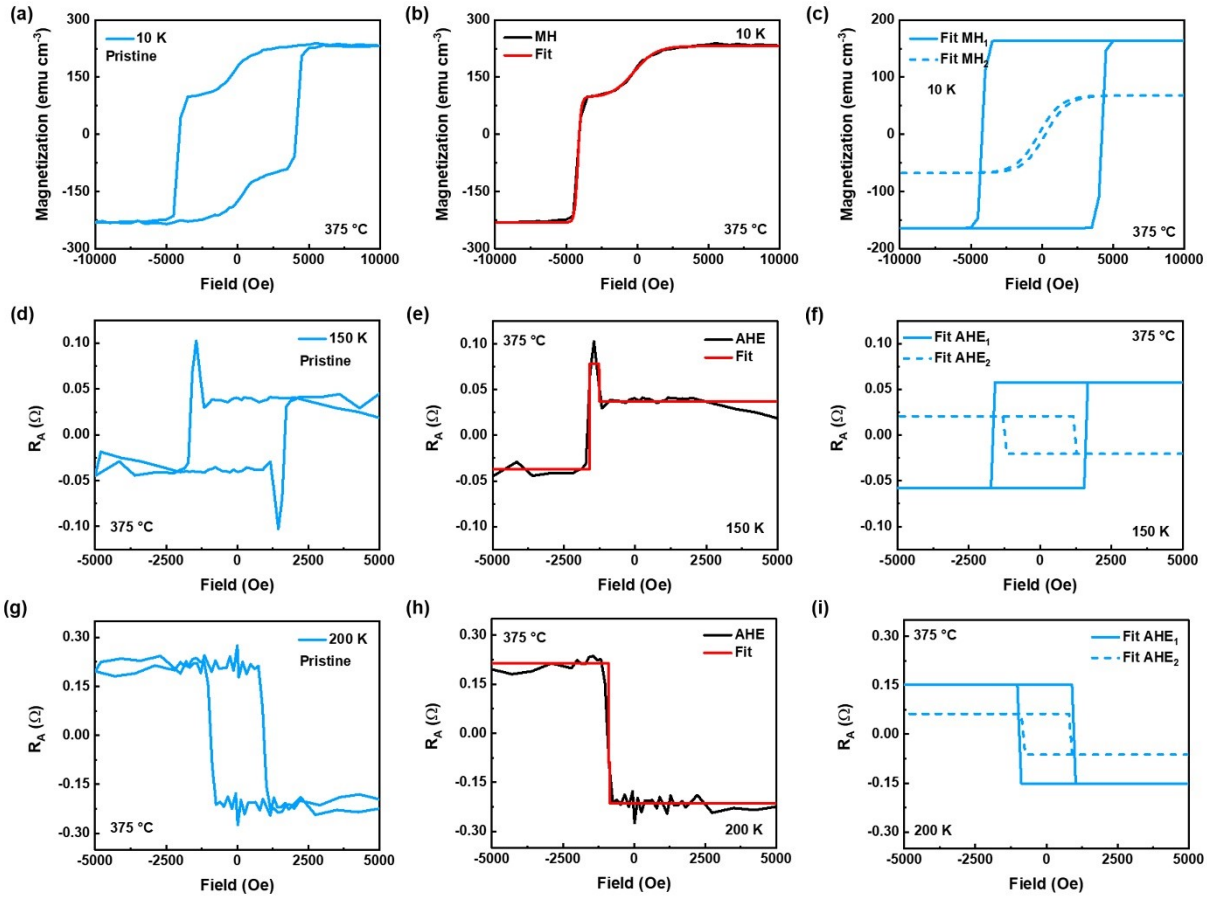

FIG. S12. Magnetic properties and AHE of NCO film. (a) Dependence of OOP magnetization on magnetic field at 10 K for 43-nm-thick NCO film deposited at 375 °C. (b) The black line is the magnetic field-dependent magnetization at 10 K by sweeping from the positive to negative magnetic field. The red line is obtained by fitting Eq. 3. (c) The two components MH_1 (solid curve) and MH_2 (dotted curve) fitted from Fig. S12(a). (d,g) AHE at 150 and 200 K for the sample grown at 375 °C, respectively. (e,h) The black lines are the magnetic field-dependent R_A by sweeping from the positive to negative magnetic field. The red lines are fitted to the Eq. 3. (f,i) The two components AHE_1 (solid curve) and AHE_2 (dotted curve) fitted from Fig. S12(d),(g).

Table III. The parameters obtained by fitting the hysteresis loop at 10 K of the 43-nm-thick NCO film grown at 375 °C from Eq. 3.

	ρ_{A_1}	H_{C_1}	H_{O_1}	ρ_{A_2}	H_{C_2}	H_{O_2}
Value	-67.83502	237.09824	-1564.04792	-163.852	4180.89447	-221.22371
Standard Error	1.19015	41.82457	64.08548	1.10218	9.89701	10.13604

The reasons for the difference between “step-like” hysteresis loops and AHE components regarding the samples prepared at higher $T_{sub.}$ are as follows. Firstly, it is only a variation in the apparent form, while the physical mechanisms are compatible. Both are related to the cation valence state and distribution of NCO films grown at higher $T_{sub.}$. Secondly, the formation of “step-like” hysteresis loops in samples prepared at higher $T_{sub.}$ is caused by the presence of non-stoichiometric NCO. The non-stoichiometric NCO and the FIM phase of NCO correspond to soft magnetic phase with small coercivity and hard magnetic phase with large coercivity, respectively, and the soft-hard magnetic coupling leads to “step-like” hysteresis loops at low temperature. However, the absence of similar phenomenon in AHE components is due to the fact that cation disorder has different effect on the magnetotransport properties than magnetism. The greater cation disorder in NCO film, the stronger impurity scattering effect. Therefore, the larger contribution to AHE of the extrinsic mechanism determined by impurity scattering, which leads to sign reversal in AHE for higher $T_{sub.}$ samples. In addition, the visual representation in AHE is the appearance of antisymmetric sharp spikes near coercive field, as shown in Fig. S12(d), consisting of the sum of two opposite-sign AHE components, where the stronger one provides the positive AHE component and the weaker one gives the negative AHE component (Fig. S12(f)).

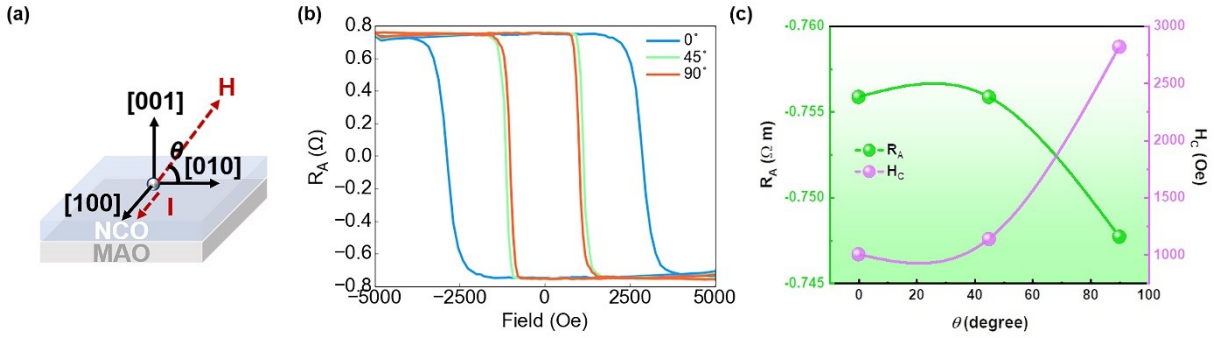

FIG. S13. Angular dependence of the AHE in NCO film. (a) Schematic of the measurement for the angle-dependent AHE. θ is the angle between the applied magnetic field and sample surface. (b) the Angle-dependent AHE at 100 K in 15-nm-thick NCO film grown at 325 °C. (c) Temperature-dependent R_A (left) and H_C (right) summarized from Fig. S13(b).

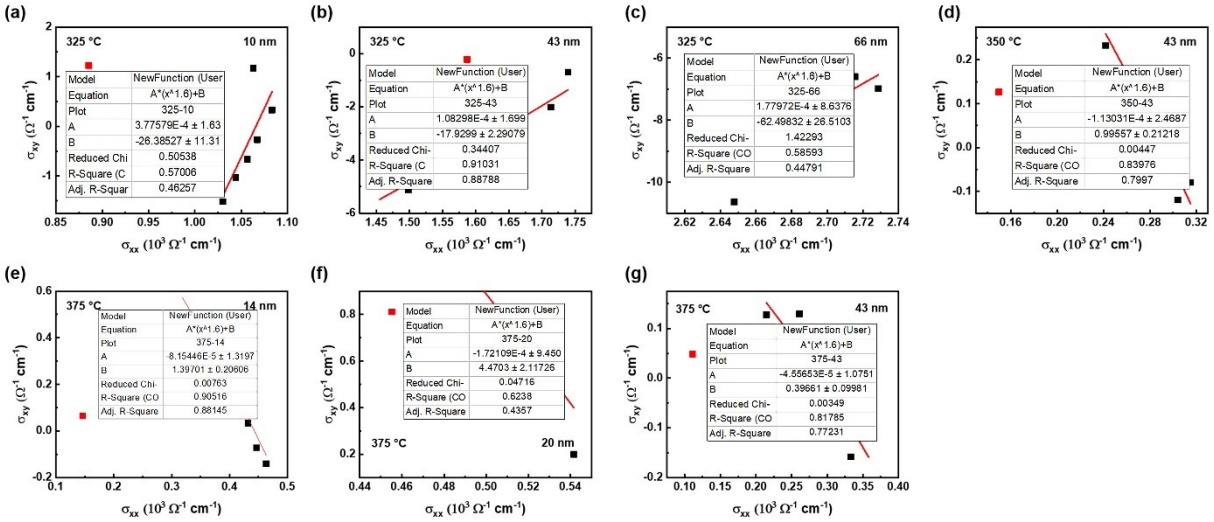

FIG. S14. Details of individual samples fitted with Eq. 4.

Due to the significant enhancement of carrier localization induced by cation disorder at low temperatures, we masked the data at 10 K during fitting process, which needs to be discussed separately. Therefore, the temperature range of the fitted data is from 50 to 300 K. In addition, the large temperature interval leads to fewer data points being obtained. However, these do not affect the fact that fitting is convergent in the high temperature region. The results indicate that the AHE consists of a combination from intrinsic mechanisms dominated by Berry curvature and extrinsic mechanisms arising from impurity scattering. The AHE of NCO films grown at 325 °C is mainly dominated by the Berry curvature, with less impact of impurity scattering. While the effect of impurity scattering in the AHE of NCO films deposited at higher $T_{sub.}$ is relatively enhanced. Next, we discuss the σ_{xy} versus σ_{xx} at 10 K. The amplitude of R_A for the sample prepared at 325 °C decreases monotonically with decreasing temperature, while that for the higher $T_{sub.}$ samples first decreases and then increases (Figs. 5(d)-(f)). While the change of R_{xx} is consistent, both are noticeably higher at low temperatures (Fig. 3(b)). Therefore, the calculated conductivity at 10 K is increased for sample prepared at 325 °C, while it is decreased for higher $T_{sub.}$ samples.

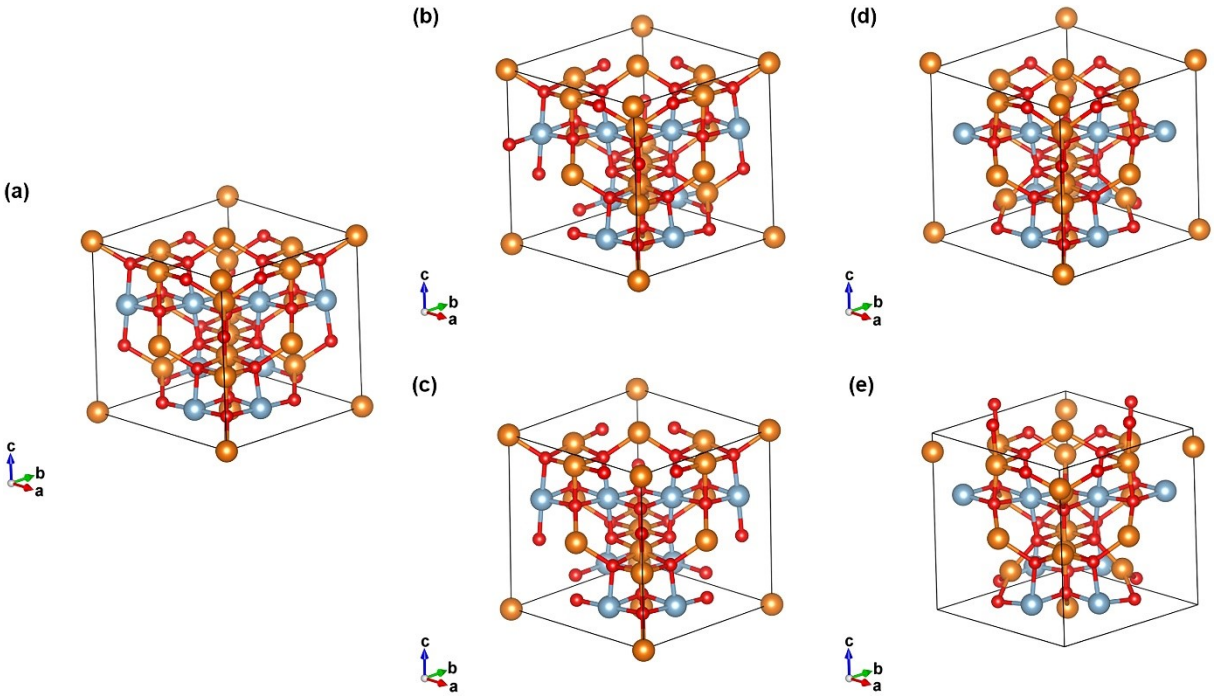

FIG. S15. Optimized crystal structures of (a) perfect inverse spinel NCO, NCO with (b) 12.5% and (c) 25% V_{Co}, as well as NCO with (d) 12.5% and (e) 25% V_O.

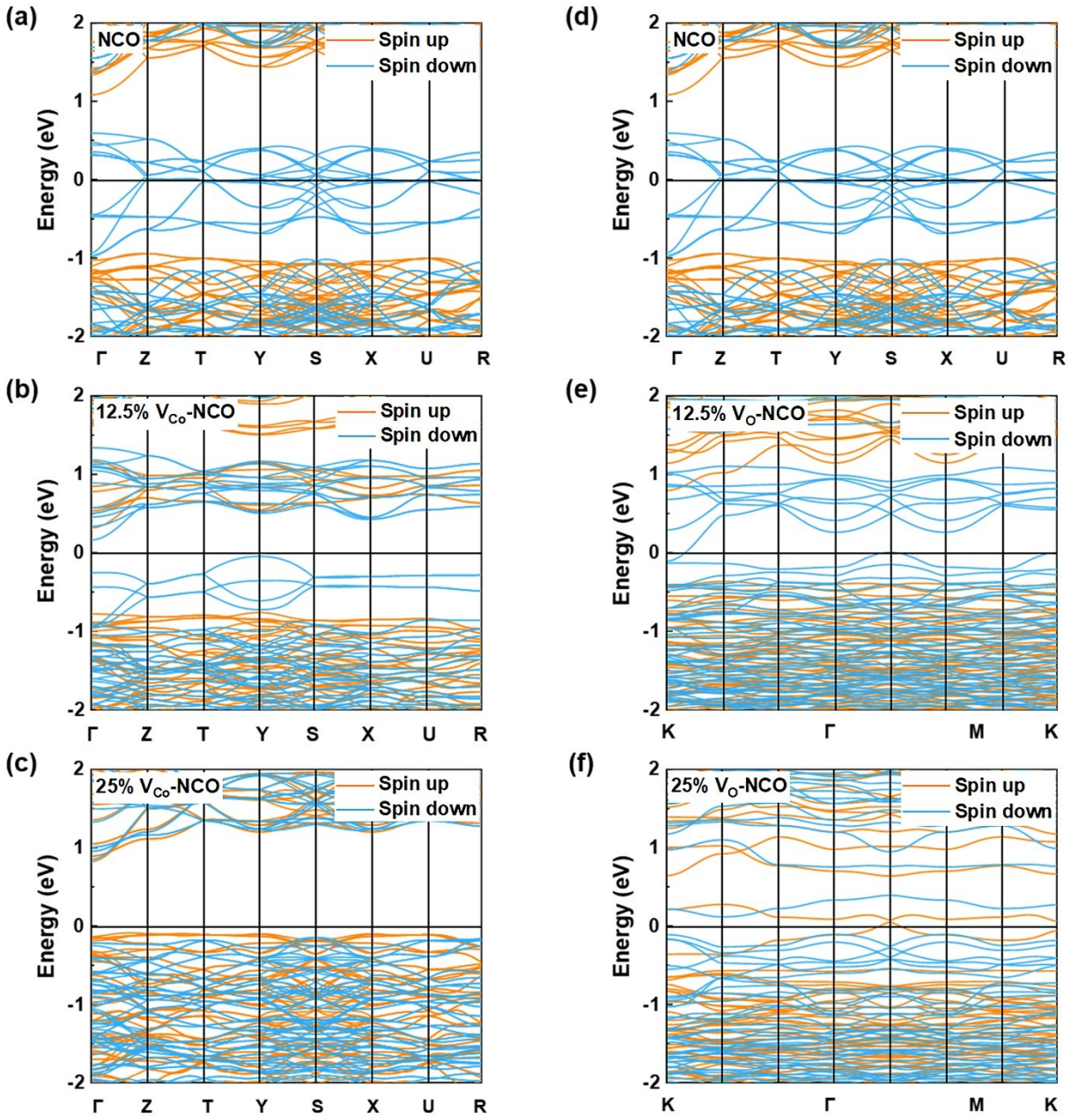

FIG. S16. Band structure of NCO films. (a-c) Band structure of perfect inverse spinel NCO, NCO with 12.5% V_{Co} and NCO with 25% V_{Co}, respectively. (d-f) Band structure of perfect inverse spinel NCO, NCO with 12.5% V_O and NCO with 25% V_O, respectively.

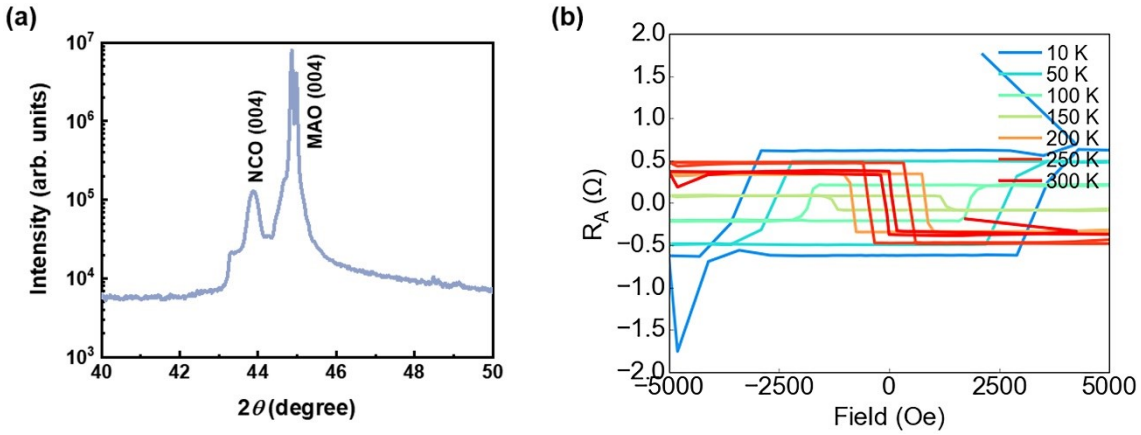

FIG. S17. Perpendicular MTJ of NCO homojunction. (a) θ-2θ XRD scans of NCO-based MTJ deposited on MAO (001) substrate. (b) The dependence of AHE on temperature for NCO-based MTJ.